Opto-Electronic Science

CN 51-1800/O4 ISSN 2097-0382 (Print) ISSN 2097-4000 (Online)

Simultaneous detection of inflammatory process indicators via *operando* dual lossy mode resonance-based biosensor

Desiree Santano, Abian B. Socorro, Ambra Giannetti, Ignacio Del Villar and Francesco Chiavaioli

Citation: Santano D, Socorro AB, Giannetti A, et al. Simultaneous detection of inflammatory process indicators via *operando* dual lossy mode resonance-based biosensor. *Opto-Electron Sci* **4**, 250005 (2025).

https://doi.org/10.29026/oes.2025.250005

Received: 25 February 2025; Accepted: 13 May 2025; Published online: 1 August 2025

Related articles

Generation of lossy mode resonances (LMR) using perovskite nanofilms

Dayron Armas, Ignacio R. Matias, M. Carmen Lopez-Gonzalez, Carlos Ruiz Zamarreño, Pablo Zubiate, Ignacio del Villar, Beatriz Romero

Opto-Electronic Advances 2024 **7**, 230072 doi: 10.29026/oea.2024.230072

Multi-resonance enhanced photothermal synergistic fiber-optic Tamm plasmon polariton tip for high-sensitivity and rapid hydrogen detection

Xinran Wei, Yuzhang Liang, Xuhui Zhang, Rui Li, Haonan Wei, Yijin He, Lanlan Shen, Yurui Fang, Ting Xu, Wei Peng

Opto-Electronic Science 2025 **4**, 240029 doi: 10.29026/oes.2025.240029

Broadband ultrasound generator over fiber-optic tip for *in vivo* emotional stress modulation

Jiapu Li, Xinghua Liu, Zhuohua Xiao, Shengjiang Yang, Zhanfei Li, Xin Gui, Meng Shen, He Jiang, Xuelei Fu, Yiming Wang, Song Gong, Tuan Guo, Zhengying Li

Opto-Electronic Science 2025 **4**, 240034 doi: 10.29026/oes.2025.240034

Smart photonic wristband for pulse wave monitoring

Renfei Kuang, Zhuo Wang, Lin Ma, Heng Wang, Qingming Chen, Arnaldo Leal Junior, Santosh Kumar, Xiaoli Li, Carlos Marques, Rui Min

Opto-Electronic Science 2024 **3**, 240009 doi: 10.29026/oes.2024.240009

More related article in Opto-Electronic Journals Group website

Opto-Electronic Science

http://www.oejournal.org/oes

OE_Journal

Website

Opto-Electronic Science

Article

October 2025, Vol. 4, No. 10

DOI: 10.29026/oes.2025.250005 CSTR: 32246.14.oes.2025.250005

Simultaneous detection of inflammatory process indicators via *operando* dual lossy mode resonance-based biosensor

Desiree Santano[1], Abian B. Socorro[1,2], Ambra Giannetti[3]*, Ignacio Del Villar[1,2]* and Francesco Chiavaioli[3]

Detecting multiple analytes simultaneously, crucial in disease diagnosis and treatment prognosis, remains challenging. While planar sensing platforms demonstrate this capability, optical fiber sensors still lag behind. An *operando* dual lossy mode resonance (LMR) biosensor fabricated on a D-shaped single-mode fiber (SMF) is proposed for quantification of clinical indicators of inflammatory process, like in COVID-19 infection. Dual LMRs, created via two-step deposition process, yield a nanostructure with distinct SnO_2 thicknesses on the flat surface of the fiber. Theoretical and experimental analyses confirm its feasibility, showing a sensitivity around 4500 nm/RIU for both LMRs. A novel insight in spatially-separated biofunctionalization of the sensitive fiber regions is validated through fluorescence assays, showcasing selectivity for different immunoglobulins. Real-time and label-free detection of two inflammatory markers, C-reactive protein and D-dimer, empowers the platform capability with a minimum detectable concentration below 1 μg/mL for both biomolecules, which is of clinical interest. This proof-of-concept work provides an important leap in fiber-based biosensing for effective and reliable multi-analyte detection, presenting a novel, compact and multi-functional analytical tool.

Keywords: fiber optic biosensors; multi-analyte detection; inflammatory process indicators; dual lossy mode resonance (LMR); label-free detection

Santano D, Socorro AB, Giannetti A et al. Simultaneous detection of inflammatory process indicators via *operando* dual lossy mode resonance-based biosensor. *Opto-Electron Sci* **4**, 250005 (2025).

Introduction

The global outbreak of COVID-19, caused by the spread of the novel coronavirus SARS-CoV-2, has posed an unprecedented challenge to public health systems worldwide[1]. The varied clinical manifestations of COVID-19, ranging from mild symptoms to severe respiratory distress and systemic complications, have paved the way for the development of robust diagnostic tools to evaluate patients based on disease severity and further clinical management of required treatments[2,3]. In this context, the identification and quantification of a pool of specific biomarkers associated with disease progression have then emerged as a critical research challenge[4–7]. Overall, an inflammatory clinical picture is also what occurs in the case of COVID-19 infection.

Among the numerous biomarkers under investigation as inflammatory process indicators, C-reactive protein (CRP) and D-dimer have earned significant attention.

[1]Electrical and Electronic Engineering Department, Public University of Navarra, Pamplona 31006, Spain; [2]Institute of Smart Cities (ISC), Public University of Navarra, Pamplona 31006, Spain; [3]Institute of Applied Physics "Nello Carrara" (IFAC), National Research Council of Italy (CNR), Sesto Fiorentino 50019, Italy.

*Correspondence: A Giannetti, E-mail: a.giannetti@ifac.cnr.it; I Del Villar, E-mail: ignacio.delvillar@unavarra.es

Received: 25 February 2025; Accepted: 13 May 2025; Published online: 1 August 2025

CRP is a biomarker associated with an acute-phase disease, which rapidly increases in response to inflammation, infection and tissue injury, making it a key indicator of the body's inflammatory response[8,9]. On the other hand, D-dimer is a degradation product of fibrin, associated with coagulation and fibrinolysis processes. Elevated levels of D-dimer have been observed in most of inflammatory processes and in severe COVID-19 cases as well, testifying an increased risk of thrombosis and vascular complications[10].

Optical fiber biosensors possess remarkable features in comparison to other biosensing platforms[11], such as the potential for *in vivo* sensing[12] and working in harsh environments[13]. Among the different sensing techniques used to develop an optical fiber biosensor, it is worth mentioning interferometric configurations[14,15], microfibers[16,17], fiber gratings[18,19] and thin-film-based structures, such as surface plasmon resonance (SPR)[20,21], localized SPR[22], Bloch surface wave[23] and lossy mode resonance (LMR)[24].

Given their remarkable features in sensing the RI changes, LMRs have been extensively studied in the last 10 years, both theoretically and experimentally[25–28], and also applied to thriving applicative scenarios[29,30]. While both SPR and LMR exploit a nanometer thin-film to endow the excited fiber modes, the generation mechanism of the LMRs stems from the mode transition from the fiber to the nanofilm, which in turn enables the interaction with the surrounding environment for sensing. This condition is fulfilled when the real part of permittivity of the nanofilm is positive and higher in magnitude than its own imaginary part, which should be as much low as possible (low material losses), and the real part of permittivity of the fiber material[31,32].

LMR-based sensors are quite versatile and powerful, leading to their proposal in numerous applications, primarily focusing on two domains. The first one is the detection when the surrounding medium is air (RI = 1), as for gas sensors[33], humidity sensors[34] or volatile organic compounds[35]. The second one is the detection in liquid samples with a refractive index (RI) ranging from 1.31 to 1.35. This includes chemical sensors for substances such as ammonia[36] or cortisol[37], sensors that permit to monitor electrochemical processes[38], and biosensors for immunoglobulin G (IgG)[24], D-dimer[39] or Tau protein[40], thus representing a reliable and effective technology platform for highly specific and real-time monitoring and quantification of clinical biomarkers, with the potential for an early diagnosis of diseases, and hence the aid in providing timely treatment strategies. However, one of the biggest challenges in sensing with optical fibers remains the potential and capability of simultaneous multi-target detection and analysis. This can be unveiled when there is a generation of multiple optical resonances that work independently. Differently from SPR-based sensing systems, LMR-based technology forecasts this option. One possibility is envisaged by increasing the thickness of the thin film that enables the generation of higher guided modes[30]. However, each resonance presents a different sensitivity, and there is a progressive reduction of the sensitivity as a function of the mode order. Moreover, it is not possible to discriminate the region in the deposited area along the fiber that refers to a specific resonance. Therefore, the device allows for detecting only a single parameter or analyte.

The possibility of multi-target detection and quantification using optical fibers still remains hidden and seen as a challenge to be achieved. The literature accounts just for two examples where optical fibers were used to detect more biological-related parameters. In 2012, Lin et al. proposed a proof-of-concept multi-window optical fiber sensor making use of multiple particle plasmon resonance of silver nanoparticles and gold nanorods deposited separately onto two distinct unclad portions of the fiber for multi-analyte detection[41]. They took advantages of time-division multiplexing method to interrogate and collect the optical signal, thus making the process slightly slower and more complex. Moreover, very standard biomolecules like biotin and streptavidin were considered and also the sensitive regions were spatially separated, thus implying larger volumes and longer binding times. Subsequently, in 2022, Zhang et al. developed an optical fiber sensing system that can be used for the continuous and real-time monitoring of four brain biomarkers simultaneously, such as brain pH, temperature, dissolved oxygen, and glucose levels[42]. The systems consisted of Y-type fiber to launch and collect light and the fiber tip was coated with a sensitive film. The sensing principle was actually based on the change in intensity of the optical signals due to the variation of absorption of the four indicators of biomarkers encapsulated in sol-gel networks. Therefore, any real and effective binding and quantification of biomolecules took place.

Here we propose an *operando* dual LMR biosensor manufactured onto a D-shaped SMF for the simultaneous detection of clinical indicators of inflammatory process,

like in COVID-19 infection. The dual LMR structure forecasts a two-step deposition process that creates a stepwise nanostructure with distinct SnO_2 thicknesses onto the flat surface of the D-shaped fiber region. This enables to have two LMRs that work independently, separated spatially and located at different wavelengths, because each region of the nanostructure is responsible for a different cut-off wavelength of the mode guided in the thin film. The spatially-separated surface biofunctionalization of the two SnO_2 nanofilms is effectively demonstrated by grafting two distinct types of IgG antibodies, each labeled with a different dye. Subsequently, the detection selectivity is verified by developing appropriate bio-assays. Fluorescence characterization confirms this revolutionary outcome. Finally, we validate the feasibility, reliability and effectiveness of the proposed multi-target biosensing platform for the selective detection of CRP and D-dimer biomarkers, as severity indicators of inflammatory process. The simultaneous and independent detection of two biomarkers at the same time with a single fiber sensor is demonstrated for the very first time in the literature thanks to a spatially-separated surface biofunctionalization, and hence the findings of this research open up novel and intriguing perspectives and possibilities with optical fiber biosensors for simultaneous multi-analyte quantification as a paradigm shift in the field.

Materials and methods

Chemicals

The methacrylic acid/methacrylate copolymer (Eudragit® L100) is purchased from Evonik Degussa GmbH (Düsseldorf, Germany). Bovine serum albumin (BSA), all the reagents for buffer preparation (phosphate-buffered saline (PBS), 10 mM, pH 7.4) and ethanol are purchased from Sigma-Aldrich (Milan, Italy). 1-Ethyl-3-[3-dimethylaminopropyl] carbodiimide hydrochloride (EDC) and N-hydroxy succinimide (NHS) are purchased from Thermo Fisher Scientific (Milan, Italy). Rabbit IgG, mouse IgG, goat anti-rabbit-IgGAlexaFluor647 (excitation peak at 650 nm and emission peak at 665 nm) and goat anti-mouse-IgGAlexaFluor488 (excitation peak at 496 nm and emission peak at 519 nm) are purchased from Life Technologies Italia (Milan, Italy). Human CRP recombinant, CRP antibody (anti CRP) clone 5 and human D-dimer antibody clone 2 are obtained from HyTest (Turku, Finland). D-dimer human protein is purchased from Sigma-Aldrich (Milan, Italy).

Numerical analysis

FIMMWAVE is utilized for simulating the D-shaped SMF. Propagation data are obtained using FIMMPROP, an integrated module within FIMMWAVE. The simulations are structured into four sections: an input SMF segment, two side-polished SMF segments (each with varying SnO_2 coating thickness), and an output SMF segment. The finite difference method (FDM) solver is selected for the SMF segment due to its recognized accuracy and precision for cylindrical waveguides. Conversely, for the side-polished SMF segment, characterized by a more complex profile, the finite element method (FEM) solver is employed. This approach makes easier the creation of a mesh with increased mesh points at the material boundaries. In both SMF sections, only one mode is taken into account, as light is exclusively guided through the core. Conversely, in the side-polished regions, 20 modes are considered to encompass the interaction between the light guided by the core mode and the modes of the cladding, resulting from polishing and subsequent deposition of nano-films.

Dual LMR manufacturing

The dual LMRs are implemented over nanocoated D-shaped fibers purchased from Phoenix Photonics LTD, UK, and consisting of a standard SMF-28 from Corning®, US, with a polished region in between. In this case, the fibers have a cladding/core diameter of 125/8 μm and the length of the polished portion is 10 mm.

In a previous study on a D-shaped fiber refractometer, two different nanoscale materials (TiO_2 and SnO_2) were used[43]. However, preliminary tests using contact angle measurements that are shown in Fig. S1 and detailed in the Supplementary information confirm that these two materials exhibit distinct properties in terms of molecular affinity to water, with SnO_2 being very hydrophilic $(37 \pm 11)°$, while TiO_2 being slightly hydrophobic $(114 \pm 1)°$ due to the deposition process. To this reason, the use of two different nano-materials is not pinpointed as the ideal condition to develop an effective dual-resonance biosensor since the adhesion of the functional layer can be envisaged to be different, as well as the biosensor response in the two different sensing regions. In addition, under repeated experimental conditions, it has been proved that SnO_2 deposited via DC sputtering adheres better to the D-shaped fiber than TiO_2 deposited via

ALD. Long-lasting biosensor experiments have sometimes experienced drifts in the optical signal due to the detachment of TiO_2 from the fiber, whereas SnO_2 has remained stable and durable. Therefore, the new dual LMR sensing configuration was finally designed and manufactured based on SnO_2 nano-films only. This guarantees the same working conditions (affinity to water, adhesion of the functional layer and biosensor response) for both the sensing regions.

Afterwards, the polished region is coated with two different nanometer-scale thicknesses of SnO_2. First, a 155 nm thick SnO_2 layer is deposited over the D-shaped fiber with a DC sputtering machine (NanoPVD, NanoVacuum, Australia). The size of the sputtering target is 50.8 mm in diameter and 3 mm in thickness. The deposition is carried out at a pressure of 1.1×10^{-1} mbar of argon and a current of 120 mA, with rotational tool operating at a speed of 1 rpm. Then, the D-shaped region is partially covered using a mask according to the methodology described in ref.[43], where a longer region is used for the LMR located at shorter wavelength in order to balance the inherent lower visibility compared to the LMR located at shorter wavelengths. Finally, 8 mm of the D-shaped region is covered with a small glass fragment serving as a mask, while the other 2 mm remains uncovered (see Fig. 1(a)). With this procedure, a second deposition of 30 nm of SnO_2 is made onto the uncovered length of the D-shaped region in order to generate two independent LMRs.

Sensitivity test

RI measurements are carried out in order to test the response of the two LMRs and then retrieve their sensitivity. With this purpose, different concentrations of glucose are dissolved in water at different dilution ratios in order to cover the RI range from 1.333 (pure water) to 1.345 RIU. Then the sensitive region of the fiber is immersed in the prepared solutions. Further details about these experiments are provided in the Supplementary information.

Selective and separated surface functionalization and its optical characterization

As stated above, the sensitive region of the sensor is 10 mm long with two different spatial regions. The first, 8 mm long and an estimated thickness of 155 nm of SnO_2, corresponds to the first LMR. The second, 2 mm long and an estimated thickness of 185 nm of SnO_2, corresponds to the second LMR. The 3D sketch of the sensor is shown in Fig. 1(a). To allow a separated surface functionalization between the two adjacent sensitive regions, and hence to make it possible the multi-analyte sensing, a proper tool and method to separately functionalize both sides are developed. Figure 1(b) shows the *ad hoc*

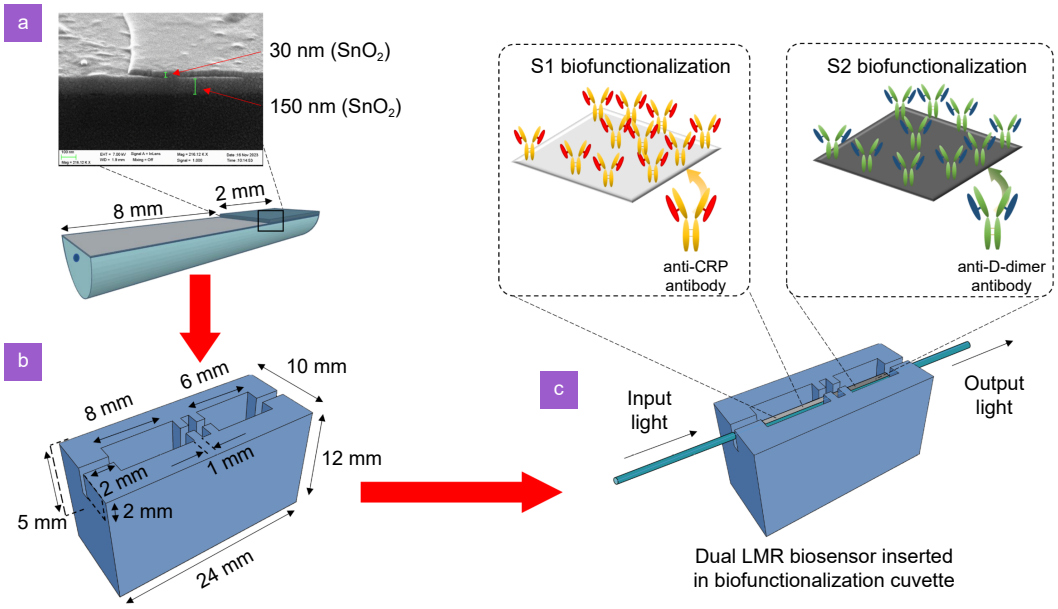

Fig. 1 | Details of the proposed dual LMR fiber biofunctionalization system. (**a**) 3D sketch of the dual LMR sensor with two different SnO_2 thicknesses on the D-shaped SMF and related SEM image. (**b**) Dimensioned sketch of the manufactured piece used for separating the two regions of the dual LMR D-shaped SMF during the separate surface functionalization. (**c**) Detail of how functionalization occurs within the cuvette in both parts of the dual LMR.

developed tool used for the purpose. It consists of a 24 mm-long cuvette with 3 wells inside that can be manufactured with a simple commercially-available 3D printer. The wells are 0.5 mm deep and feature grooves at the edges and in the middle. This allows the fiber to be inserted while ensuring it remains covered with the correct solution, which is not transferred between the wells. The wells at the edges are long enough to cover the two sensitive portions of the fiber, while in the central area there is a 1 mm well that prevents mixing the solutions of the border wells, thus shielding each other.

As depicted in the top inset of Fig. 1(a), the characterization of the nanostructure fabricated onto the D-shaped SMF surface, featuring two distinct SnO_2 thicknesses, is conducted utilizing an atomic force microscope (AFM) equipped with RTESPA probes in tapping mode from Bruker Innova. Additionally, a scanning electron microscope (SEM), specifically the UltraPlus FESEM model from Carl Zeiss Inc., is employed with an in-lens detector operating at 3 kV and an aperture diameter of 30 μm for further analysis.

Experimental setup

The transmission spectrum of the fiber sensors is monitored using the experimental setup shown in Fig. 2, together with the microfluidic system where the fiber sensor is placed during the bioassay experiments. Light is injected through a wide-spectrum multi-LED light source (FibreLabs, Inc., SLD-1310/1430/1550/1690). Between the broadband source and the fiber sensor, there is an in-line polarizer and a polarization controller, which enable the control and adjustment of the polarization of light travelling within the D-shaped SMF with either TE (or s-polarized) or TM (p-polarized) polarized signals. The output of the fiber is linked to an optical spectrum analyzer (OSA, Anritsu MS9030A-MS9701B), allowing real-time monitoring of the transmission spectrum in a wavelength range from 1200 nm to 1700 nm.

As detailed in a previous publication[44], the microfluidic system comprises two identical sections, each of 23 mm in width, 10 mm in depth, and 100 mm in length, constructed from polyetherimide (ULTEM resin, top bar) and stainless steel (bottom bar). In between of the two bars, a micro-channel measuring 1 mm × 1 mm × 50 mm is engraved, resulting in a total volume of 50 μL. The dimensions of the micro-channel are optimized for the precise manipulation of small volume samples.

In real world applications, temperature changes may have an impact on the sensor response. However, in our case, the detection of target analytes occurs inside a microfluidic system with embedded temperature stabilization[39,40]. Two Peltier cells (23 mm × 25 mm) are inserted beneath the stainless steel bar. The temperature control is achieved through the use of a thermistor located within a lateral aperture in the same stainless steel bar that acts as a feedback element of a control unit (TEC controller, LDC-3722B, ILX Lightwave), ensuring precise thermal regulation within the microfluidic channel. This configuration enables to guarantee very stable conditions (±0.05 °C) in terms of environmental changes in long-term experiments, thus making negligible the temperature cross-sensitivity. Finally, during the bioassay experiments, the solutions are accurately injected inside the microfluidic channel at predefined flow rates via a

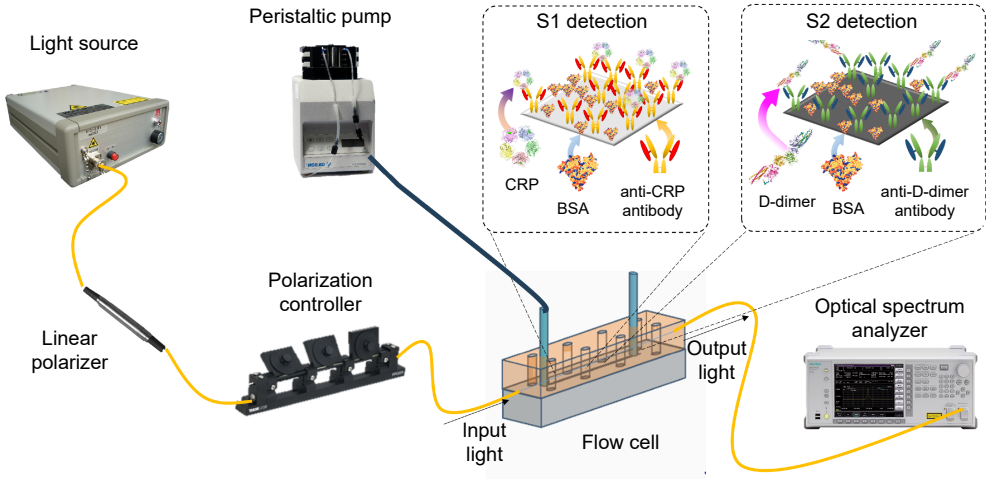

Fig. 2 | Complete experimental setup employed for the bioassay implementation, together with the microfluidic system. The detection of the analytes, D-dimer and CRP, occurs within the flow cell.

peristaltic pump (GILSON Minipulse 3; Middleton, WI, US) and suitable medical-grade tubing.

Bioassay protocol

After the optical characterization of the D-shape SMF with dual LMR in terms of volume RI sensitivity[45], the platform is used to detect biomolecules and clinical biomarkers. In the first test, rabbit and mouse IgGs are selected in order to assess the viability of the biosensing system. Afterwards, two clinical biomarkers involved in the diagnosis of COVID-19 severity, D-dimer and CRP proteins, are simultaneously detected following the bioassay protocol described here below.

First, the entire sensing surface of the optical fiber is functionalized with Eudragit® L100 as previously reported[24,29]. After that, the –COOH groups provided by the functional layer are activated in the cuvette by means of EDC (40 mg/mL) and NHS (6 mg/mL) cross-linking chemistry for 20 min. The solution is removed and the sensitive region is washed three times with PBS. The solution containing the biorecognition element is then added in the corresponding well of the cuvette for its immobilization onto the fiber surface, as it is shown in Fig. 1(c). The biofunctionalization process would add some complexity that may hinder the scalability of the sensing platform. However, this process can be automatized by integrating robotic handling for fiber insertion into the cuvette and subsequent solution injection, thus making it feasible for large-scale applications.

In the case of workability of the cuvettes and the proof-of-concept test for spatially selective biorecognition element immobilization, 500 μg/mL of goat anti-rabbit-IgG^{AlexaFluor647} and of goat anti–mouse–IgG^{AlexaFluor488} are directly added in the respective well for 1 h, then rinsed with PBS. The fluorescence measurements are performed with Zeiss Axio Observer Fluorescence Microscopy System using 5×, 0.12 N.A. objective lens, and Colibri source system (Zeiss, Oberkochen, Germany). In the case of subsequent bioassays involving label-free IgGs, 1 mg/mL is the concentration of both rabbit and mouse IgGs spiked in PBS that is added in the respective well. For the experiments involving COVID-19-related biomarkers, anti CRP and anti D-dimer antibodies are used in 500 μg/mL concentration spiked in PBS and added in the respective well, for 1 h. After that, the surface is rinsed in PBS to remove unreacted biorecognition elements.

At this point, the fiber is then glued and sealed into the closed microfluidic system as illustrated in the experimental setup shown in Fig. 2, and a constant temperature of 30 °C is maintained throughout each experiment. Once inside, PBS is injected in the microfluidic channel until reaching a stable optical signal. Subsequently, a blocking solution containing BSA is introduced in a concentration of 0.1 mg/mL spiked in PBS, and with a further rinsing in PBS in order to remove any unreacted biomolecule and then obtain the biosensor baseline before the analyte detection. All rinsing steps are carried out at a flow rate of 50 μL/min.

In the detection part, increasing concentrations of the analytes are injected for 15 minutes at a flow rate of 25 μL/min and the biosensor surface is rinsed in PBS after each analyte injection until the stabilization of the optical signal is attained. The concentrations of the analyte in IgG-related experiments are 1, 10 and 100 μg/mL of anti-rabbit IgG and anti-mouse IgG. In the case of the bioassays for the detection of CRP and D-dimer proteins, the concentrations used are 1, 5, 10, 50, 100 μg/mL. In all cases, the analyte is spiked in the same running buffer (PBS).

Results and discussion

In pursuit of advancing optical biosensing technologies, this study successfully addresses to the very first time the challenge of envisaging, developing, characterizing, and assessing a novel dual LMR sensor manufactured onto a D-shaped SMF for dual-analyte biosensing. Creating dual LMRs using SnO_2 nano-films is essential for detecting multiple biomarkers simultaneously with optical fiber devices. This involves a precise two-step deposition process to generate a nanostructure with varying SnO_2 thicknesses on the flat region of the D-shaped SMF. Verification through numerical analysis and microscopy-based measurements, including AFM and SEM, confirms the accuracy of the fabrication.

Optical characterization of dual LMR sensing configuration

As stated in the introduction, multiple LMRs within a single sensor can be obtained by increasing the thickness of the one-layer nanocoating[46]. However, these resonances are interdependent in their spectral shifts, limiting their suitability for sensing only one parameter at a time. This issue can be overcome by the deposition of a nanostructure with varying thicknesses of thin film onto the flat surface of a D-shaped SMF[43]. The first step is to

study the optimal conditions for manufacturing the SnO_2-based dual LMR sensor numerically. Figure 3(a) shows the simulation window in the cross section of the D-shaped fiber. This simplification permits to reduce the computation, enabling the generation of corresponding fields and spectra in a more efficient manner. Figure 3(b) shows the optical field intensity of the fundamental fiber mode ($HE_{1,1}$) at 1580 nm, the central resonance wavelength for the region deposited with 185 nm, where the evanescent field can be clearly distinguished in the boundary of the fiber cladding and the SnO_2 thin film. In addition, Fig. 3(c) shows one-dimensional plots at X=0 from Fig. 3(b), illustrating the evolution of the optical field intensity across both regions. This observation reveals that the evanescent field reaches its peak intensity at 1310 nm for the 155 nm coated region and at 1580 nm for the 185 nm coated region.

The Supplementary information section provides further details on the numerical analysis. In particular, Figs. S2 and S3 account for the evolution of the core mode along with the fundamental mode of the cladding, and permit to observe the increase of the evanescent field when the cladding mode is guided in the thin film, according to LMR theory[28]. In addition, in Fig. S4(a) the simulation of the transmission spectra can be visualized with two minima at 1310 nm and at 1580 nm that agree with the optical field intensity values observed in Fig. 3(c). Figure S4(a) also shows the wavelength shift of both bands as a function of the surrounding medium RI, which agrees well with the experimental results of Fig. S4(b). Finally, in Fig. S5 it is possible to observe the real time evolution of the signal during the experiment, with a sensitivity in both LMRs of 4500 nm/RIU (see Fig. S5(c)).

The effect of functionalization with Eudragit® L100 has also been investigated. It is expected to have a

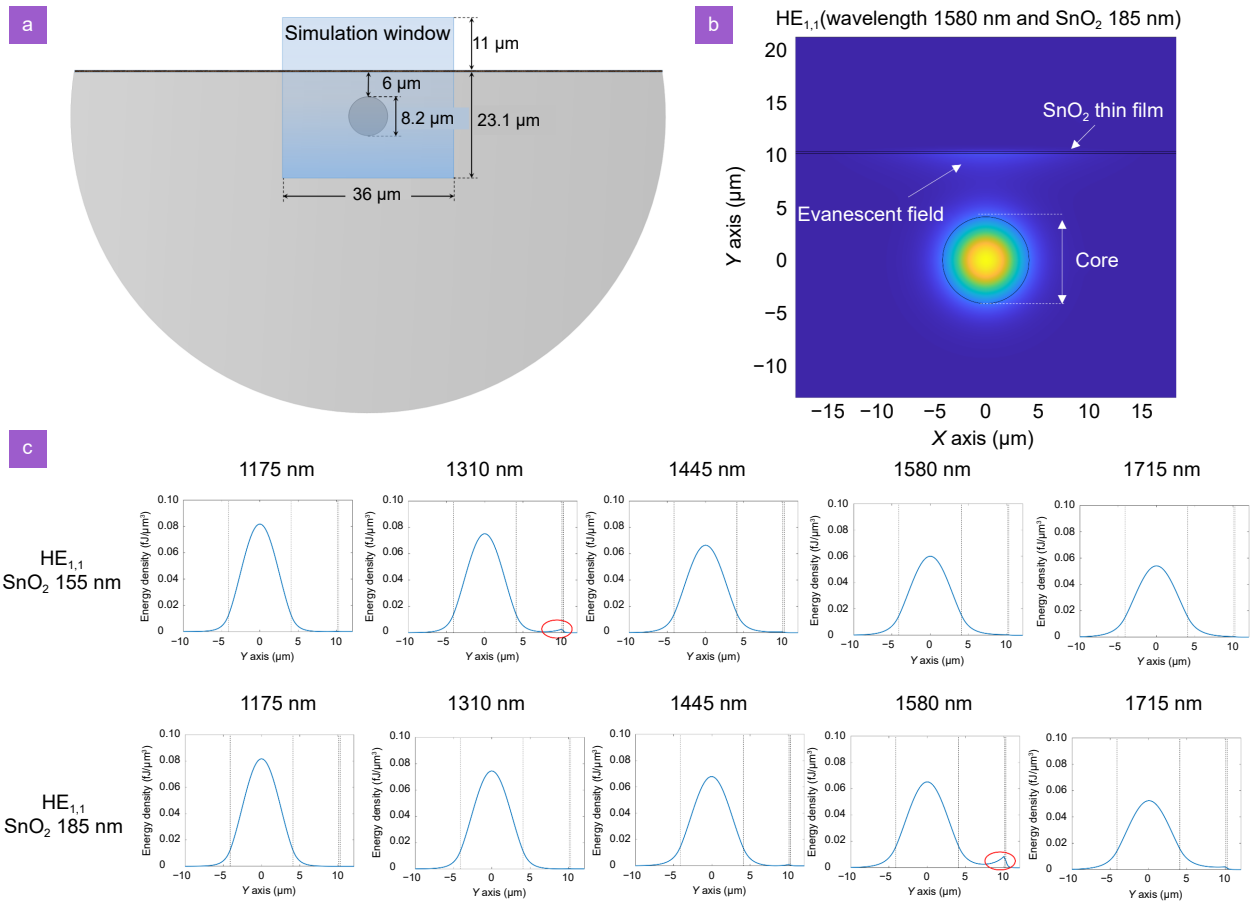

Fig. 3 | Optical field intensity in the cross section D-shaped fiber cross section. (**a**) Schematic with the simulation window in the center of the figure. (**b**) Optical field intensity of $HE_{1,1}$ fiber mode in the transversal section of the 185 nm SnO_2 nano-film deposited onto one of the two D-shaped fiber regions. The 1580 nm wavelength is the central wavelength of the corresponding LMR. (**c**) Optical field intensity of $HE_{1,1}$ for X=0 in (b) as a function of wavelength. Both the 155 nm and the 185 nm coated regions are shown. The red circles indicate the evanescent field at the resonance wavelengths of 1310 nm and 1580 nm for the 155 nm and 185 nm coatings, respectively.

negligible impact on the sensor sensitivity since the functional layer has a mean thickness less than 60 nm and a RI slightly more than that of silica composing optical fibers. These conditions do essentially not change the guiding properties of fiber modes and, ultimately, have no impact on the sensor performance. In order to confirm this claim, some simulations in terms of wavelength shift using the D-shaped fiber sensor of ref.[24] uniformly coated with a 160 nm thick SnO_2 film are performed with and without Eudragit layer, when immersing it in liquid of RI of 1.333 and another liquid with slightly higher RI of 1.343. The curves shown in Fig. S6 detail a wavelength shift around 50 nm in both cases, thus retrieving a sensitivity around 5000 nm/RIU in agreement with the experimental one. Further details can be found in Supplementary information.

Figure 4(a) illustrates the spectra of the two-step manufacturing process. The position of the second LMR agrees well with the simulations, while the first LMR is shifted around 100 nm compared to the simulations. This is due to the fact that for the simulations thickness values are taken from the fabrication of the sensor onto a glass slide in order to assess the thicknesses of the nanofilms at each deposition step. Afterwards, the sample undergoes the characterization with AFM (Bruker Innova with RTESPA probes in tapping mode). Figure 4(b) displays an image of the glass slide utilized in AFM, displaying the distinguishable colors of the two sensing regions, perceptible even to the naked eye. AFM measurements corroborate a 155 nm thick film of SnO_2 following the initial deposition, followed by an additional 30 nm thick film of SnO_2 to achieve a total thickness of 185 nm for the second region. This configuration facilitates the realization of the dual LMR sensing platform, as illustrated in Fig. 4(c) and 4(d). In particular, Fig. 4(c) presents an AFM measurement highlighting the contrast between the 155 nm thick SnO_2 region and the bare region without any deposition. This step represents the first of the two-steps deposition process to attain a dual LMR sensor. Figure 4(d) presents an AFM measurement with the aim of highlighting and assessing the second step of the deposition process by comparing the 155 nm thick SnO_2 region with the 185 nm thick SnO_2 region. In addition, Table 1 gathers the main parameters of the AFM analysis, such as the average thickness, the mean roughness and the root mean square roughness of the two deposited regions. These values are in agreement with those previously reported in ref.[47].

Experimental assays with IgG

After the previous experiments, the next step is to envision and test an optical label-free biosensor for the detection of two distinct analytes at the same time. The biggest challenge is to functionalize the two sensing regions of the D-shaped fiber independently. This has been achieved through the design of a custom-made cuvette depicted Materials and methods (Fig. 1(b)), which enables the grafting of various biorecognition elements onto both sensing regions, minimizing or entirely eliminating cross-interaction**.** The initial test is carried out directly immobilizing anti-rabbit-IgG^{AlexaFluor647} and anti-mouse-IgG^{AlexaFluor488} as they are well-known and cost-effective biomolecules. The use of labeled antibodies with two different dyes has been selected to prove the grafting of distinct biorecognition elements in the two sensing regions of the fiber. It is worth underlining that the excitation wavelengths are at 647 nm related to red colored light for the anti-rabbit IgG and at 488 nm related to green colored light for the anti-mouse IgG. Figure 5(a) displays some pictures taken with the Zeiss Axio Observer Fluorescence Microscopy System using the mosaic wide-area modality. From the top to the bottom, it is shown the fluorescence image of the dual functionalized fiber in color and in black & white (gray scale from 0 to 255) when both the excitation wavelengths are active, and also when the single excitation wavelength is alternatively active. From Fig. 5(a), it is possible to distinguish the two different fiber regions with labeled anti-rabbit IgG (right) and anti-mouse IgG (left) with a very small overlapping region of a length of roughly 1 mm highlighted in light yellow. In addition, from the fluorescence images in black & white, it is possible to appreciate a good degree of uniformity and homogeneity in the surface coverage of antibodies grafted onto the fiber. The fluorescence images with the single excitation wavelength active are further processed using Fiji Imagej imaging tool in order to extract additional features.

Figure 5(b) and 5(d) depict a 3D plot of the fluorescence signal, represented in gray levels, focusing on the fiber portion where the deposition of anti-mouse IgG and anti-rabbit IgG is most uniform. The regions with uniform deposition of anti-mouse IgG are highlighted in green, while those with uniform deposition of anti-rabbit IgG are highlighted in red. Moreover, Fig. 5(c) and 5(e) report the fluorescence profile (gray level vs. longitudinal distance expressed in μm) taken along the selected fiber portions. As confirmed by the calculated mean

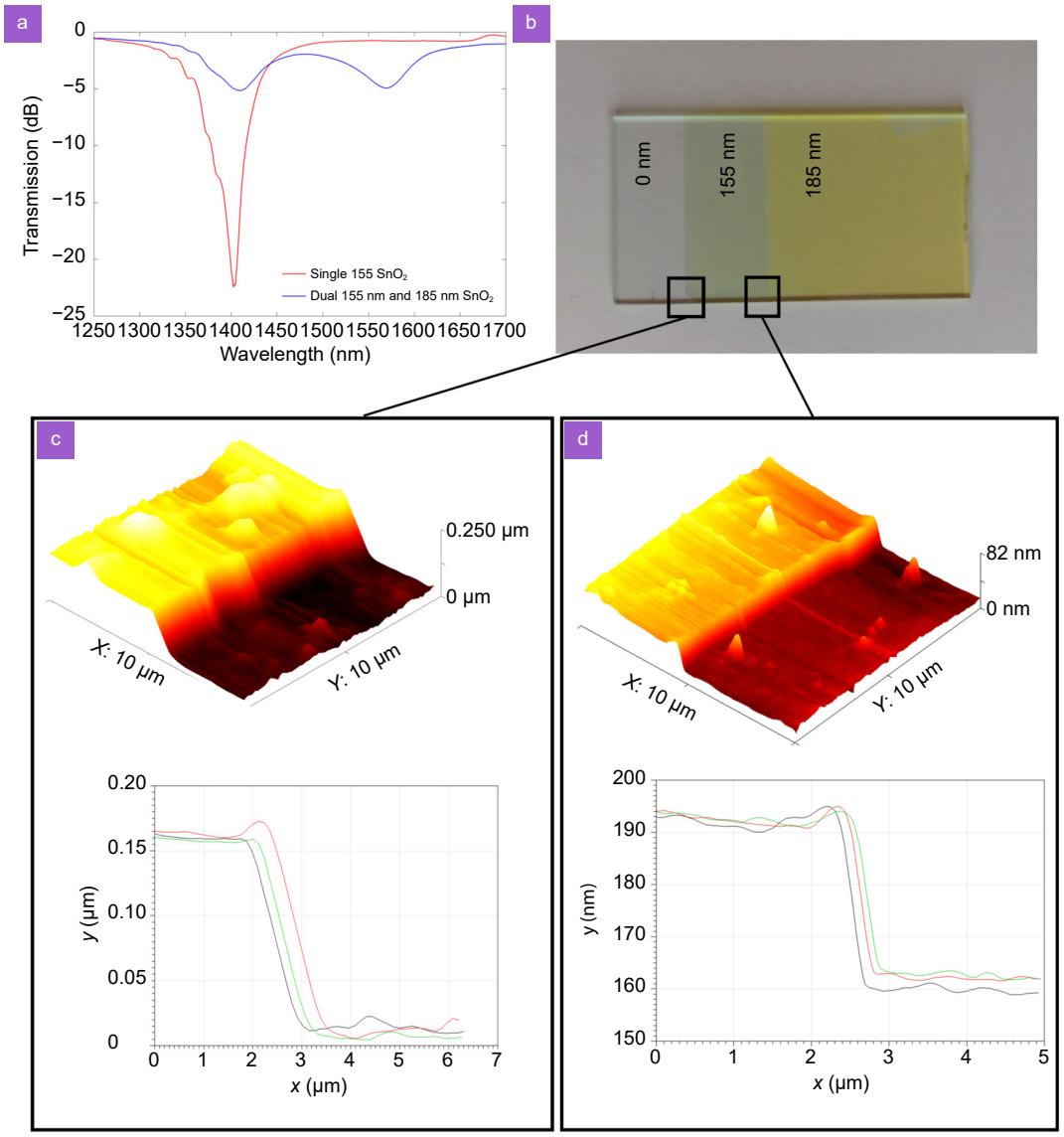

Fig. 4 | Optical characterization of SnO_2-based dual LMR sensing configuration manufactured onto D-shaped SMF. (**a**) Spectra of the dual LMR sensor obtained after the first and second depositions of SnO_2 nano-films. (**b**) Glass slide deposited following the same method of fiber sensor for the purpose of AFM measurements. (**c**) AFM measurement after the first SnO_2 deposition. (**d**) AFM measurement after the second SnO_2 deposition.

Table 1 | Statistical parameters from AFM images.

	Average thickness (nm)	Roughness (nm)	
		Root mean square	Mean
SnO_2 (155 nm)	159.633	3.348	2.172
SnO_2 (185 nm)	188.871	2.938	1.889

value of the gray level in the two fiber portions, even if the region related to the anti-mouse IgG details a higher gray level and a better homogeneity than the other related to the anti-rabbit IgG, the values are still comparable and remarkable considering a fluorescence background noise of 10 ± 10.

After assessing the spatially selective immobilization of the biorecognition element onto the two different areas of the fiber, the complete immunoassay was carried out. Starting from the immobilization of the mouse IgG and rabbit IgG onto the two different areas of the fiber as previously described, the next step consists of placing the sensor inside the microfluidic system, where all solutions pass through both regions of the dual D-shaped

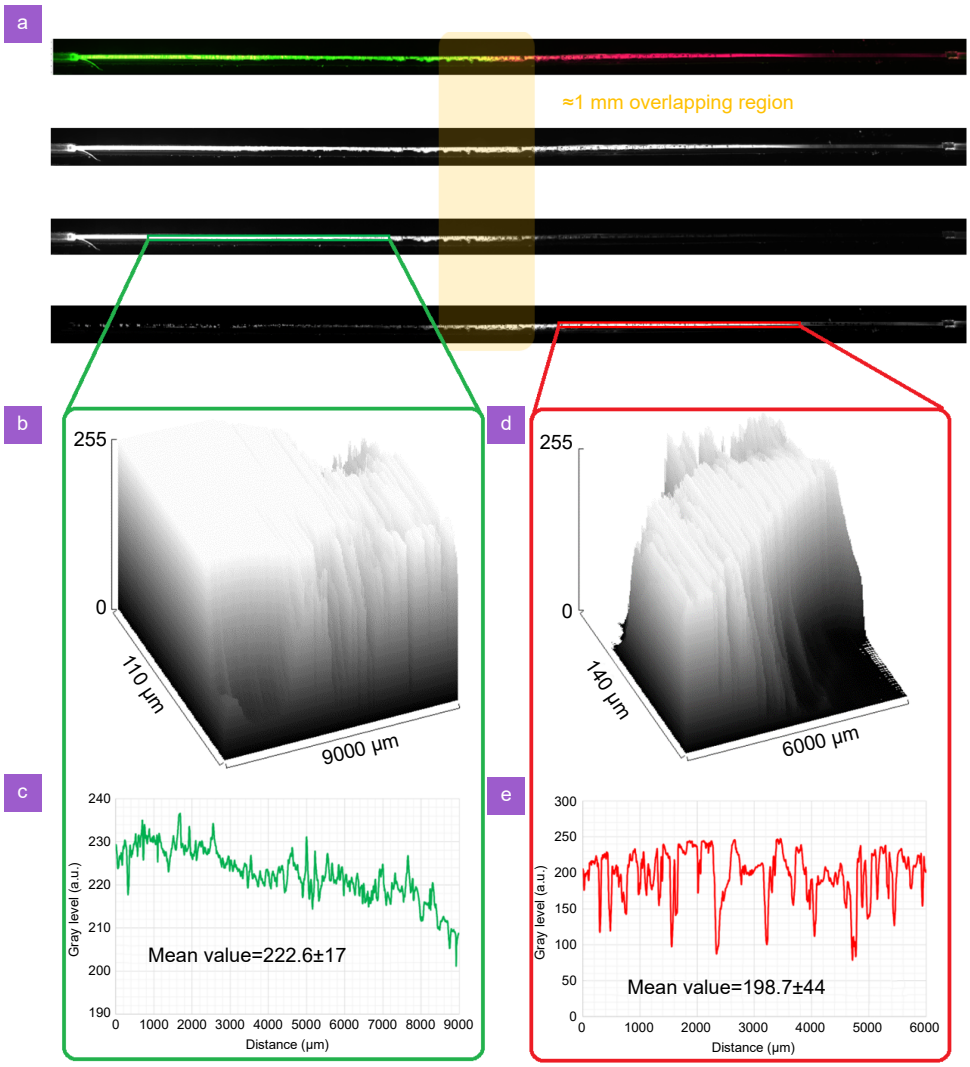

Fig. 5 | Verification of the viability of separated surface functionalization via fluorescence image showcasing the separation of the two sensing regions of the fiber where two distinct labeled antibodies are grafted (goat anti-mouse-IgG^{AlexaFluor488} and goat anti-rabbit-IgG^{AlexaFluor647}, left and right respectively). (**a**) Fluorescence images of the dual functionalized fiber in color and in black & white (gray scale from 0 to 255) from the top to the bottom when both the excitation wavelengths are active, and also when the single excitation wavelength is alternatively active. Dimension of fluorescence mosaic image: 500 μm (height) x 12000 μm (width). (**b**) The 3D plot of the fluorescence signal expressed in gray level considering the fiber portion where there is the most uniform deposition of the anti-mouse IgG highlighted in green and (**c**) related fluorescence profile (gray level vs. longitudinal distance expressed in μm) taken along the same fiber portion. (**d**) The 3D plot of the fluorescence signal expressed in gray level considering the fiber portion where there is the most uniform deposition of the anti-rabbit IgG highlighted in red and (**e**) related fluorescence profile (gray level vs. longitudinal distance expressed in μm) taken along the same fiber portion.

SMF. In the bioassay implementation, solutions of both analytes (anti-mouse IgG and anti-rabbit IgG) are alternately injected from the lowest concentration to the highest one. This way ensures that all concentrations of both analytes interact with both sensing regions of the fiber. Figure 6 shows the complete sensorgram during the detection of both analytes, where it is possible to point out that each analyte is only detected with one of the two LMRs. This further confirms the effectiveness and the reliability of the method in terms of separation of both areas during the immobilization of the biorecognition element, as already demonstrated in fluorescence (Fig. 5).

In particular, the LMR at shorter wavelengths enables the detection of anti-mouse-IgG, while the LMR at longer wavelengths allows the detection of anti-rabbit-IgG. The same concentration range from 1 μg/mL to 100 μg/mL has been selected for both analytes. Ideally, the response in the sensorgram should be almost flat in one of the two sensing regions when the injected analyte binds

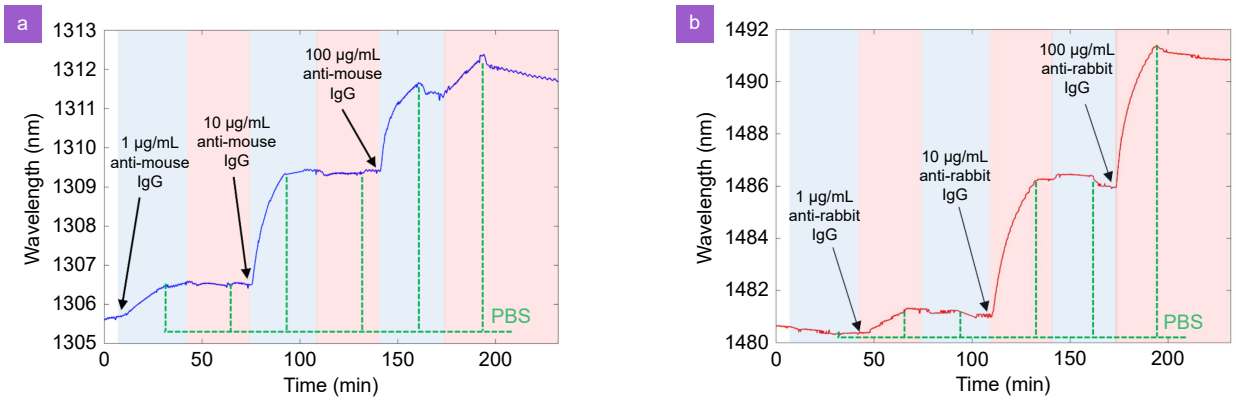

Fig. 6 | Sensorgrams related to the detection of two different analytes during a single bioassay and using a single optical fiber sensor. (**a**) Detection of three different concentrations of anti-mouse-IgG with the LMR located at shorter wavelengths. (**b**) Detection of three different concentrations of anti-rabbit-IgG with the LMR located at longer wavelengths.

with the biorecognition element grafted on the other sensing region, and vice versa. This helps to unveil any cross-selectivity between the two analytes. However, it is important to highlight that at a high concentration of the analyte (for instance, 100 μg/mL in Fig. 6) the optical signal in the sensorgram related to the sensing region placed close to the inlet of the microfluidic system (Fig. 6(a)) suffers from a slight influence from the other analyte (Fig. 6(b)). This implies that the analyte present in the injected solution, upon contact with the first sensing region, tends to accumulate therein. Hence, anti-rabbit-IgG slightly modifies the optical signal of anti-mouse-IgG. However, this unwanted signal drops down during the subsequent rinsing step without changing the level of the baseline taken in PBS, guaranteeing the absence of any effective cross-selectivity binding interaction.

Experimental assays with CRP and D-dimer

Once the feasibility of the proposed dual-analyte optical fiber biosensor has been confirmed through the detection of two IgGs, the same biosensing platform is envisaged for the detection of clinically relevant biomarkers. The serological value of both CRP and D-dimer has been associated within a biomarker pool indicating the severity of COVID-19 infection. Figure 7 illustrates the sensorgrams and calibration curves achieved through the detection of both proteins. The detection of CRP (Fig. 7(a)) is carried out using the LMR located at shorter wavelengths, while D-dimer protein (Fig. 7(c)) is monitored with the LMR placed at longer wavelengths, generated with the deposition of thicker SnO_2 nano-film. The concentration range used in the detection of both proteins goes from 1 μg/mL to 100 μg/mL and the minimum detectable concentration is undoubtedly below 1 μg/mL in both cases, which is of clinical interest for inflammatory processes and early stages of COVID-19 infection due to systemic inflammation[48,49].

The effect seen in Fig. 6 also occurs during the detection of CRP and D-dimer (Fig. 7). In particular, the optical signal in the D-dimer sensorgram (Fig. 7(c)) follows the trend of the optical signal during the CRP injection (Fig. 7(a)) like an accumulation occurring in the non-specific sensing region. As happening in experiments involving IgGs, this condition barely affects the signal baseline of D-dimer, since the optical signal primarily recovers during the rinsing step in PBS, and hence without affecting the overall biosensing performance of the proposed biophotonic platform. It is worth underscoring that all the experiments are carried out by flowing the two different target analytes on both sensitive regions of the fiber where the specific biorecognition element (i.e., anti-mouse IgG or anti-rabbit IgG antibodies, and anti-CRP or anti-D-dimer antibodies) has previously been grafted. Therefore, each experiment can be figured out as the specificity test with non-target analytes since each represents the non-target analyte of the other. However, the sensorgrams in Figs. 6 and 7 reveal minor signal change in the non-target regions during the analyte injection at high concentrations. In fact, it represents just a small fraction of the total shift observed during the injection of the corresponding target analyte. In the case of IgG (mouse and rabbit) detection, the maximum percentage in the detection error due to the non-target analyte is (6 ± 1)% occurring at 100 μg/mL. When dealing with more complex molecules like CRP and D-dimer, this error rises up to (11 ± 1)% (a more complete analysis

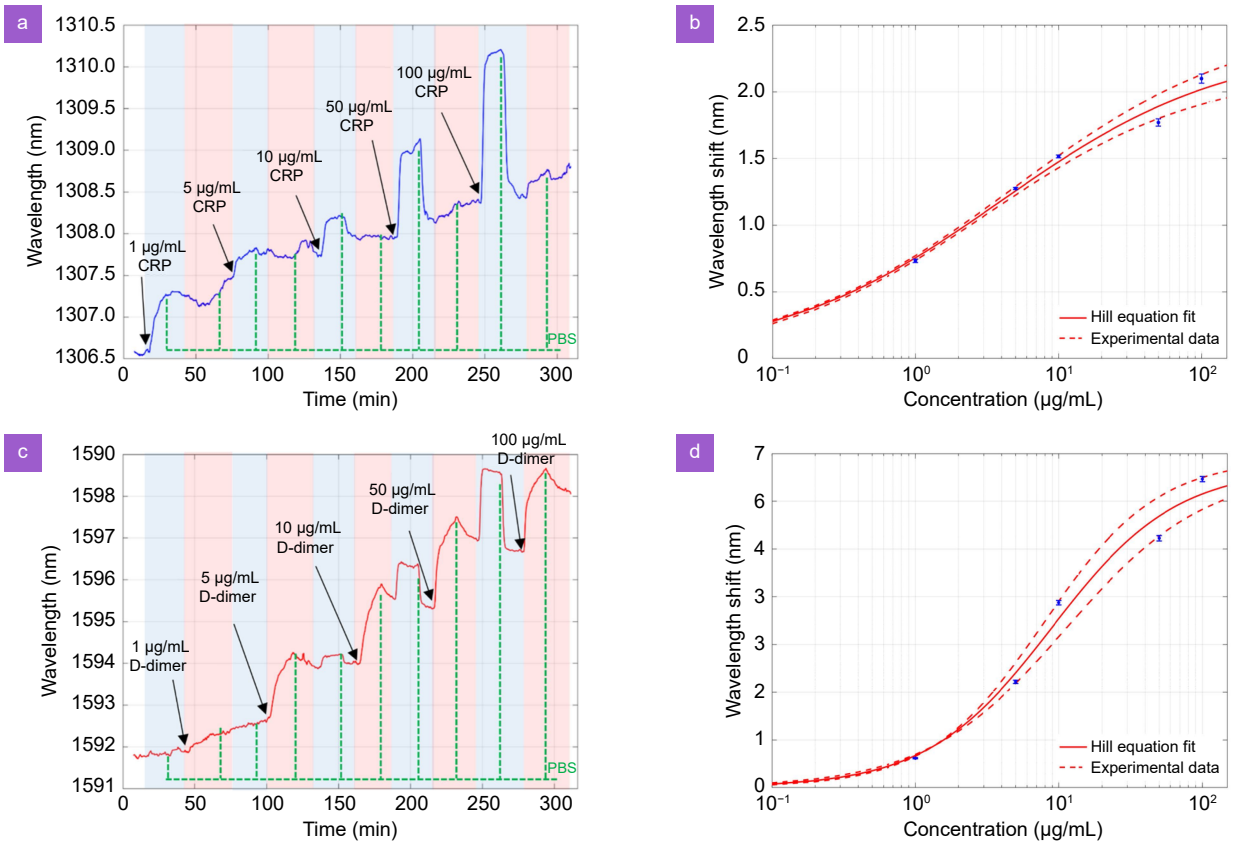

Fig. 7 | Sensorgrams and calibration curves related to the detection of CRP and D-dimer proteins. (**a**) Sensorgram and (**b**) related calibration curve achieved during the detection of different concentrations of CRP protein with the LMR at shorter wavelengths. (**c**) Sensorgram and (**d**) related calibration curve achieved during the detection of different concentrations of D-dimer protein with the LMR at longer wavelengths. In the calibration curves of CRP (b) and D-dimer (d), the continuous red line accounts for the fitting curve obtained from the Hill equation, whereas the dashed red lines determine the 99% confidence level noise band by taking into account the deviation of residuals from the respective fitting curves.

is reported in Supplementary information, as well as in Tables S1 and S2). However, the cross-interference can be envisaged when working with different biomolecules flowing within the same microfluidic channel, since it is almost impossible to have any cross-interference or to have any cross-affinity among different biorecognition elements.

Figure 7(b) and 7(d) detail the calibration curves of CRP and D-dimer proteins, respectively. The CRP response saturates earlier, exhibiting a smaller change in the optical signal in comparison to the D-dimer one. Conversely, the D-dimer response shows a higher wavelength shift, with a higher concentration of the analyte required for reaching the saturation. This different behavior can probably be explained by the fact that the molecular weight of D-dimer (180 kDa) is greater than that of CRP (23 kDa). In these calibration curves, the experimental data points are fitted using the Hill function (continuous red lines) and the R^2 correlation coefficient is 0.994 for CRP and 0.992 for D-dimer. The Hill equation, a widely recognized mathematical expression, is employed to quantitatively assess the extent of interaction among ligand binding sites[50]. Following the guidelines set by the International Union of Pure and Applied Chemistry (IUPAC), this equation also enables the calculation of the limit of detection (LoD) from the attained calibration curves[51,52]. The LoD obtained for the CRP protein is 0.013 μg/mL, while the one for the D-dimer is 0.221 μg/mL, which are values of clinical significance to discriminate the COVID-19 severity even at early stages[9,53]. In addition, the 99% confidence level noise band depicted as dashed red lines is shown by taking into account the deviation of residuals from the respective fitting curves. While the standard deviation of experimental points provides an indication of the overall noise of the system during the detection, the mentioned noise band leverages the effectiveness, reliability and reproducibility of the experimental results. In addition, it is

worth noting that the noise bands in Fig. 7(b) and 7(d) for both CRP and D-dimer target analytes detail a negligible deviation from the respective fitting curves at low concentrations, thereby enhancing the achieved LoDs. Conversely, a larger deviation occurs at high concentrations where the effect of cross-interference of multiple analytes would probably contribute to this phenomenon.

Although the LoD is one of the most representative performance parameter of biosensors, it is indeed a parameter that is closely related to the specific characteristics of the target analyte, thus making a direct comparison between different biosensors very challenging. In addition, CRP and D-dimer are not among the most commonly used biomarkers in optical fiber biosensing[11]. Nevertheless, some optical fiber biosensors have reported CRP detection, such as a polydopamine nanospheres-modified SPR biosensor that has attained a LoD of 0.22 μg/mL[54]. An even lower LoD around 2.4×10^{-5} μg/mL[55] has recently been reported using a localized SPR biosensor combined with hybrid Au@Ag nanostructures. As far as D-dimer is concerned, an LMR-based biosensor implemented on a D-shaped fiber has demonstrated a LoD of 10 ng/mL[39]. However, those examples are just restricted to the optimization of the sensitivity of the biosensor, but none of them underscore a multiparametric biosensor capable of detecting more than one single analyte at a time on a single fiber, as demonstrated in the present proof-of-concept work.

Clearly, there are other multi-analyte RI-sensing systems, essentially based on SPR. For instance, Vala M. et al. have proposed a sensor for the detection up to 10 analytes but not using optical fibers as platform[56], while several optical-fiber based multichannel sensing configurations are mentioned in ref.[57]. In contrast, one of the main advantages of LMR-based sensors is that they can be generated with less expensive materials than noble metals used for SPR-based sensors. Another advantage lies in its versatility and potential scalability, as recent findings have demonstrated its capability for translation onto planar substrates[58], and even to photonic integrated circuits[59], which dramatically increases the potential of the concept of LMR-based multiparameter sensing shown here. Moreover, our LoDs fit well with clinical values. In a clinical setting where different biomarkers like CRP are associated with fast progression and worse prognosis in COVID-19 infection, it is known that patients with CRP level greater than 41.8 μg/mL are more likely to develop severe disease[9]. Moreover, Zhang et al. recently establish that the optimum cut-off value of D-dimer to predict in-hospital mortality is 2.0 μg/mL with a sensitivity of 92.3% and a specificity of 83.3%[53].

In this work, purified biomarkers in PBS have been used, and a validation with spiked complex samples (i.e., plasma or serum) would certainly enhance translational relevance. However, the goal of this work is demonstrating the capability to spatially distinguish one biomarker to the other even along close sensitive regions. Therefore, this can be envisaged an essential technological proof-of-concept of multi-window optical biosensor implemented on a D-shaped fiber. In fact, the outcomes obtained with the present study would have the capability to differentiate between the groups with better and worse prognosis during the COVID-19 infection, thus conferring a valuable tool for early identification, personalized treatment, and better prognosis. In addition, real time monitoring of changes in the optical properties occurring on the sensor surface provides a dynamic and immediate insight into biomolecular interactions, surpassing the limitations of conventional detection methods. Additionally, being label-free, this biosensing platform eliminates the need for chemical labels or tags, streamlining the detection process and minimizing potential interference and costs.

Finally, the ability to unbind target analytes from their respective biorecognition elements —thus enabling regeneration of the biosensing layer—is an important aspect for the real-world deployment of biosensors. It has been demonstrated[24] that the use of a solution of 1% sodium dodecyl sulfate (SDS) can unbound the target analyte from the biosensing surface. This protocol works very well in case of antibodies used as biorecognition element. Moreover, the potential to regenerate LMR-based optical fiber biosensors has recently been emphasized through the use of an alternative functionalization approach combining silanization with an acid regeneration buffer[59].

Conclusions

This study presents a pioneering dual lossy mode resonance (LMR) biosensor fabricated on a D-shaped single-mode optical fiber (SMF) for real-time and label-free detection of two analytes. The development of dual LMRs through a precise two-step SnO_2 deposition process has been experimentally validated, demonstrating a high refractive index sensitivity of approximately 4500 nm/RIU for both resonances. Verification through numerical

analysis and microscopy-based measurements, including AFM and SEM, confirms the accuracy of the fabrication.

The second challenge to overcome is the independent functionalization of two distinct sensing regions over an optical fiber. With a custom-developed holder and an *ad hoc* assay protocol, we have successfully detected two different immunoglobulins G (IgGs) using the dual LMR sensing configuration. The implementation of a fluorescence-based assay provides the unambiguous evidence of the effective separation of the two sensing regions over the D-shaped fiber in terms of specific surface functionalization. In addition, the optical results confirm the separated surface functionalization in two distinct areas with a negligible overlapping of the biorecognition elements that turns out into a complete and clear selectivity in the detection of multiple analytes. This novel proof-of-concept in surface functionalization represents an important leap in fiber-based biosensing for multi-analyte detection.

Once the capability of the biosensor for independent dual analyte detection was established, it was subsequently evaluated for the simultaneous quantification of two clinically relevant inflammatory biomarkers, CRP and D-dimer proteins. The sensor enabled precise identification and quantification of both CRP and D-dimer, achieving a LoD for CRP of 0.013 μg/mL, while the one for the D-dimer was 0.221 μg/mL. These values are below their clinical cut-off values for assessing COVID-19 severity, thereby reinforcing its applicability in biomedical applications.

However, the proposed biosensing system might have constraints that should be underscored. First, considering the operating spectral range (1250–1700 nm), the length of the sensitive region of the D-shaped fiber (10 mm) and the bandwidth of each generated LMR (50 nm on average), no more than three independent sensitive fiber regions can effectively be envisaged, which in turn enables the simultaneous detection of three biomarkers at the most on a single fiber sensor. Second, this design finely works when medium-size biorecognition elements like antibodies or similar (molecular weight > 15 kDa). Therefore, there might be some issues in terms of cross-affinity and cross-interference when dealing with small-size biorecognition elements like nanoantibodies, enzymes or aptamers. The same argument can be translated to the target analyte to be detected. Finally, considering a typical spectrum of the dual-LMR fiber sensors with not so deep optical resonances (less than 10 dB), this has a clear impact on the sensor resolution and detection accuracy, which in turn determine the system noise and, ultimately, the LoD, altough this can be solved with deeper polishing of the D-shaped fiber, allowing for stronger resonances and enhanced performance.

To conclude, the proposed optical fiber-based platform offers a versatile and compact analytical tool for dual-target biosensing, with broad implications for biomedical research and clinical diagnostics. In addition, the label-free nature and real-time monitoring capabilities of the sensor provide significant advantages over conventional diagnostic methods, eliminating the need for chemical labels while enhancing sensitivity and specificity. Hence, the dual LMR biosensor represents a significant advancement in optical fiber biosensing technology, paving the way for the development of next generation multiparametric detection systems with high sensitivity, specificity, and clinical relevance.

References

1. Filip R, Gheorghita Puscaselu R, Anchidin-Norocel L et al. Global challenges to public health care systems during the COVID-19 pandemic: a review of pandemic measures and problems. *J Pers Med* **12**, 1295 (2022).
2. National Institutes of Health. COVID-19 Treatment Guidelines Panel. Coronavirus Disease 2019 (COVID-19) Treatment Guidelines. Available at https://www.covid19treatmentguidelines.nih.gov/.
3. Pandey SK, Mohanta GC, Kumar V et al. Diagnostic tools for rapid screening and detection of SARS-CoV-2 infection. *Vaccines* **10**, 1200 (2022).
4. Vandenberg O, Martiny D, Rochas O et al. Considerations for diagnostic COVID-19 tests. *Nat Rev Microbiol* **19**, 171–183 (2021).
5. Karkan SF, Baladi RM, Shahgolzari M et al. The evolving direct and indirect platforms for the detection of SARS-CoV-2. *J Virol Methods* **300**, 114381 (2022).
6. Klebes A, Ates HC, Verboket RD et al. Emerging multianalyte biosensors for the simultaneous detection of protein and nucleic acid biomarkers. *Biosens Bioelectron* **244**, 115800 (2024).
7. Thompson IAP, Saunders J, Zheng LW et al. An antibody-based molecular switch for continuous small-molecule biosensing. *Sci Adv* **9**, eadh4978 (2023).
8. Mosquera-Sulbaran JA, Pedreañez A, Carrero Y et al. C-reactive protein as an effector molecule in COVID-19 pathogenesis. *Rev Med Virol* **31**, e2221 (2021).
9. Liu F, Li L, Xu MD et al. Prognostic value of interleukin-6, C-reactive protein, and procalcitonin in patients with COVID-19. *J Clin Virol* **127**, 104370 (2020).
10. Rueda-Camino JA, Sendín-Martín V, Joya-Seijo MD et al. Plasma D-dimer value corrected by inflammatory markers in patients with SARS-CoV-2 infection: its prognostic value in the diagnosis of venous thromboembolism. *Med Clin (Barc)* **158**, 265–269 (2022).
11. Socorro-Leránoz AB, Santano D, Del Villar I et al. Trends in the

design of wavelength-based optical fibre biosensors (2008–2018). *Biosens Bioelectron X* **1**, 100015 (2019).
12. Zhou BQ, Fan KK, Guo JJ et al. Plug-and-play fiber-optic sensors based on engineered cells for neurochemical monitoring at high specificity in freely moving animals. *Sci Adv* **9**, eadg0218 (2023).
13. Yin MJ, Gu BB, An QF et al. Recent development of fiber-optic chemical sensors and biosensors: mechanisms, materials, micro/nano-fabrications and applications. *Coord Chem Rev* **376**, 348–392 (2018).
14. Betancur-Ochoa JE, Minkovich VP, Montagut-Ferizzola YJ. Special photonic crystal modal interferometer for highly sensitive biosensing. *J Lightwave Technol* **35**, 4747–4751 (2017).
15. Cardona-Maya Y, Socorro AB, Del Villar I et al. Label-free wavelength and phase detection based SMS fiber immunosensors optimized with cladding etching. *Sens Actuators B Chem* **265**, 10–19 (2018).
16. Sun DD, Guo T, Ran Y et al. *In-situ* DNA hybridization detection with a reflective microfiber grating biosensor. *Biosens Bioelectron* **61**, 541–546 (2014).
17. Li HT, Huang YY, Hou GH et al. Single-molecule detection of biomarker and localized cellular photothermal therapy using an optical microfiber with nanointerface. *Sci Adv* **5**, eaax4659 (2019).
18. Zu LJ, Wang XC, Liu P et al. Ultrasensitive and multiple biomarker discrimination for Alzheimer's disease via plasmonic & microfluidic sensing technologies. *Adv Sci* **11**, e2308783 (2024).
19. Ribaut C, Loyez M, Larrieu JC et al. Cancer biomarker sensing using packaged plasmonic optical fiber gratings: towards *in vivo* diagnosis. *Biosens Bioelectron* **92**, 449–456 (2017).
20. Liu LH, Zhang XJ, Zhu Q et al. Ultrasensitive detection of endocrine disruptors via superfine plasmonic spectral combs. *Light Sci Appl* **10**, 181 (2021).
21. Wang BT, Wang Q. Sensitivity-enhanced optical fiber biosensor based on coupling effect between SPR and LSPR. *IEEE Sens J* **18**, 8303–8310 (2018).
22. Lee B, Park JH, Byun JY et al. An optical fiber-based LSPR aptasensor for simple and rapid in-situ detection of ochratoxin A. *Biosens Bioelectron* **102**, 504–509 (2018).
23. Del Villar I, Gonzalez-Valencia E, Kwietniewski N et al. Nanophotonic crystal D-shaped fiber devices for label-free biosensing at the attomolar limit of detection. *Adv Sci* **11**, e2310118 (2024).
24. Chiavaioli F, Zubiate P, Del Villar I et al. Femtomolar detection by nanocoated fiber label-free biosensors. *ACS Sens* **3**, 936–943 (2018).
25. Batchman TE, McWright GM. Mode coupling between dielectric and semiconductor planar waveguides. *IEEE Trans Microw Theory Tech* **30**, 628–634 (1982).
26. Marciniak M, Grzegorzewski J, Szustakowski M. Analysis of lossy mode cut-off conditions in planar waveguides with semiconductor guiding layer. *IEE Proc J (Optoelectron)* **140**, 247–252 (1993).
27. Andreev A, Pantchev B, Danesh P et al. A refractometric sensor using index-sensitive mode resonance between single-mode fiber and thin film amorphous silicon waveguide. *Sens Actuators B Chem* **106**, 484–488 (2005).
28. Del Villar I, Zamarreño CR, Hernaez M et al. Lossy mode resonance generation with indium-tin-oxide-coated optical fibers for sensing applications. *J Lightwave Technol* **28**, 111–117 (2010).
29. Chiavaioli F, Janner D. Fiber optic sensing with lossy mode resonances: applications and perspectives. *J Lightwave Technol* **39**, 3855–3870 (2021).
30. Del Villar I, Arregui FJ, Zamarreño CR et al. Optical sensors based on lossy-mode resonances. *Sens Actuators B Chem* **240**, 174–185 (2017).
31. Del Villar I, Hernaez M, Zamarreno CR et al. Design rules for lossy mode resonance based sensors. *Appl Opt* **51**, 4298–4307 (2012).
32. Elosua C, Arregui FJ, Del Villar I et al. Micro and nanostructured materials for the development of optical fibre sensors. *Sensors* **17**, 2312 (2017).
33. Usha SP, Mishra SK, Gupta BD. Fiber optic hydrogen sulfide gas sensors utilizing ZnO thin film/ZnO nanoparticles: a comparison of surface plasmon resonance and lossy mode resonance. *Sens Actuators B Chem* **218**, 196–204 (2015).
34. Bohorquez DL, Del Villar I, Corres JM et al. Generation of lossy mode resonances in a broadband range with multilayer coated coverslips optimized for humidity sensing. *Sens Actuators B Chem* **325**, 128795 (2020).
35. Elosua C, Arregui FJ, Zamarreño CR et al. Volatile organic compounds optical fiber sensor based on lossy mode resonances. *Sens Actuators B Chem* **173**, 523–529 (2012).
36. Tiwari D, Mullaney K, Korposh S et al. An ammonia sensor based on Lossy Mode Resonances on a tapered optical fibre coated with porphyrin-incorporated titanium dioxide. *Sens Actuators B Chem* **242**, 645–652 (2017).
37. Usha SP, Shrivastav AM, Gupta BD. A contemporary approach for design and characterization of fiber-optic-cortisol sensor tailoring LMR and ZnO/PPY molecularly imprinted film. *Biosens Bioelectron* **87**, 178–186 (2017).
38. Śmietana M, Sobaszek M, Michalak B et al. Optical monitoring of electrochemical processes with ITO-based lossy-mode resonance optical fiber sensor applied as an electrode. *J Lightwave Technol* **36**, 954–960 (2018).
39. Zubiate P, Urrutia A, Zamarreño CR et al. Fiber-based early diagnosis of venous thromboembolic disease by label-free D-dimer detection. *Biosens Bioelectron X* **2**, 100026 (2019).
40. Chiavaioli F, Rivero DS, Del Villar I et al. Ultrahigh sensitive detection of tau protein as Alzheimer's biomarker via microfluidics and nanofunctionalized optical fiber sensors. *Adv Photonics Res* **3**, 2200044 (2022).
41. Lin HY, Huang CH, Huang CC et al. Multiple resonance fiber-optic sensor with time division multiplexing for multianalyte detection. *Opt Lett* **37**, 3969–3971 (2012).
42. Zhang YQ, Hu YB, Liu Q et al. Multiplexed optical fiber sensors for dynamic brain monitoring. *Matter* **5**, 3947–3976 (2022).
43. Imas JJ, Zamarreño CR, Zubiate P et al. Twin lossy mode resonance on a single D-shaped optical fiber. *Opt Lett* **46**, 3284–3287 (2021).
44. Chiavaioli F, Biswas P, Trono C et al. Towards sensitive label-free immunosensing by means of turn-around point long period fiber gratings. *Biosens Bioelectron* **60**, 305–310 (2014).
45. Chiavaioli F, Gouveia CAJ, Jorge PAS et al. Towards a uniform metrological assessment of grating-based optical fiber sensors: from refractometers to biosensors. *Biosensors* **7**, 23 (2017).
46. Del Villar I, Zamarreño CR, Hernaez M et al. Generation of lossy mode resonances with absorbing thin-films. *J Lightwave Technol* **28**, 3351–3357 (2010).

47. Fuentes O, Goicoechea J, Corres JM et al. Generation of lossy mode resonances with different nanocoatings deposited on coverslips. *Opt Express* **28**, 288–301 (2020).
48. Becher Y, Goldman L, Schacham N et al. D-dimer and C-reactive protein blood levels over time used to predict pulmonary embolism in two COVID-19 patients. *Eur J Case Rep Intern Med* **7**, 001725 (2020).
49. Zhu JY, Ji P, Pang JL et al. Clinical characteristics of 3062 COVID-19 patients: a meta-analysis. *J Med Virol* **92**, 1902–1914 (2020).
50. Kurganov BI, Lobanov AV, Borisov IA et al. Criterion for Hill equation validity for description of biosensor calibration curves. *Anal Chim Acta* **427**, 11–19 (2001).
51. Long GL, Winefordner JD. Limit of detection. A closer look at the IUPAC definition. *Anal Chim Acta* **55**, 712A–724A (1983).
52. Shrivastava A, Gupta V. Methods for the determination of limit of detection and limit of quantitation of the analytical methods. *Chron Young Sci* **2**, 21 (2011).
53. Zhang LT, Yan XS, Fan QK et al. D-dimer levels on admission to predict in-hospital mortality in patients with COVID-19. *J Thromb Haemost* **18**, 1324–1329 (2020).
54. Cao GX, Chang PX, Zhang AL et al. A polydopamine nanospheres modified fiber optic SPR biosensor for specific detection of C-reactive protein. *Opt Fiber Technol* **80**, 103468 (2023).
55. Phuong NTT, Anh DT, Thao NHN et al. Application of hybrid Au@Ag nanostructures in fiber optic biosensor for rapid detection of C-reactive protein. *Opt Mater* **143**, 114184 (2023).
56. Vala M, Chadt K, Piliarik M et al. High-performance compact SPR sensor for multi-analyte sensing. *Sens Actuators B Chem* **148**, 544–549 (2010).
57. Zhang SQ, Han B, Zhang YN et al. Multichannel fiber optic SPR sensors: realization methods, application status, and future prospects. *Laser Photon Rev* **16**, 2200009 (2022).
58. Matias IR, Del Villar I, Corres JM. Lossy mode resonance-based sensors in planar configuration: a review. *IEEE Sens J* **23**, 6397–6405 (2023).
59. Santano D, Zubiate P, Socorro-Leránoz AB et al. Regenerable LMR-based fiber optic immunosensor with a SnO_2 metallic oxide thin film for label-free detection. *Talanta* **287**, 127658 (2025).

Acknowledgements

I.D.V. acknowledges financial support from the Spanish Agencia Estatal de Investigación (AEI) through project PID2023-149895OB-I00. D.S. also acknowledges a predoctoral research grant from the Public University of Navarra. F.C. acknowledges financial support under the National Recovery and Resilience Plan (NRRP), Mission 4, Component 2, Investment 1.1, Call for tender No. 1409 published on 14.9.2022 by the Italian Ministry of University and Research (MUR), funded by the European Union – NextGenerationEU – Project Title "Fiber optics sensors as a platform for cancer diagnosis and in vitro model testing" – CUP B53D23024170001 - Grant Assignment Decree No. 1383 adopted on 01/09/2023 by the Italian MUR.

Author contributions

Desiree Santano: investigation, writing-original draft, writing-review and editing. Abian B. Socorro: methodology, supervision, writing-review and editing. Ambra Giannetti: methodology, supervision, investigation, writing-review and editing. Ignacio Del Villar: conceptualization, methodology, theory analysis, supervision, writing-review and editing. Francesco Chiavaioli: conceptualization, methodology, supervision, funding acquisition, writing-review and editing.

Competing interests

The authors declare no competing financial interests.

Supplementary information

Supplementary information for this paper is available at https://doi.org/10.29026/oes.2025.250005

Scan for Article PDF